Time-delayed interactions on acoustically driven bubbly screens

Yuzhen Fan, Haisen Li, Daniel Fuster

Time-delayed interactions on acoustically driven bubbly screens

Yuzhe Fan,[1, a)] Haisen Li,[1, b)] and Daniel Fuster[2, c)]

[1)] *Acoustic Science and Technology Laboratory, Harbin Engineering University, Harbin 150001, China*

[2)] *Sorbonne Universités, UPMC Univ Paris 06, CNRS, UMR 7190, Institut Jean Le Rond d'Alembert, F-75005 Paris, France*

(Dated: 5 November 2021)

We discuss the influence of compressibility effects including time delays on the dynamics of acoustically excited bubbly screens. In the linear regime we show that the proposed model for the infinite bubbly screen recovers the results predicted by the effective medium theory up to the second order without introducing any fitting parameter when the wavelength is large compared to the inter-bubble distance. However, the effect of boundaries on finite bubbly screens is shown to lead to the appearance of multiple local resonances and characteristic periodic structures that limit the applicability of the effective medium theory. In addition a local resonance phenomenon in the liquid spacings between bubbles is observed for both infinite and finite bubbly screens with crystal structures, these effects vanishing as the crystal structure is perturbed. In the non-linear regime, we treat the current model with time-delay effects as a delay differential equation that is directly solved numerically. We show the appearance of an optimal distance for subharmonic emission for crystal structures and discuss the accuracy of effective medium theory in the strong non-linear regime.

[a)] Also at: College of Underwater Acoustic Engineering, Harbin Engineering University, Harbin 150001,China
[b)] Also at: Key Laboratory of Marine Information Acquisition and Security(Harbin Engineering University), Ministry of Industry and Information Technology, Harbin 150001, China
[c)] fuster@dalembert.upmc.fr

I. INTRODUCTION

The dynamics of cavities in liquids has attracted a lot of interest over the past few decades (Fuster, 2019; Lohse, 2018). The oscillation of an isolated bubble is well described by the Rayleigh-Plesset (RP) like equation that accounts for compressibility effects (Gilmore, 1952; Keller and Miksis, 1980; Lauterborn and Kurz, 2010; Prosperetti *et al.*, 1986). However, bubbles often appear in ensembles, and bubble-bubble interactions need to be accounted as the bubble interface acceleration influences the pressure distribution in the bubble surroundings. One traditional way to account for the influence of interactions is to use the effective medium method. Foldy (1945), Caflisch *et al.* (1985), and Commander and Prosperetti (1989) consider the influence that the dynamic bubble response have on the effective properties of a wave propagating in a bubbly liquid. The multiple interactions among bubbles are described by the interaction between each bubble and the averaged pressure field. However these models are limited to diluted systems and frequencies for which the wavelength is larger than the characteristic bubble radius and the inter-bubble distance.

In an attempt to generalize the range of applicability of these theories to shorter wavelengths and capture more accurately the interaction mechanisms among bubbles, some authors propose to solve a coupled system of RP like equations (Fan *et al.*, 2020b; Fuster and Colonius, 2011; Ilinskii *et al.*, 2007; Mettin *et al.*, 1997). These approaches can be eventually coupled with an Eulerian–Lagrangian approach (Fuster and Colonius, 2011; Maeda and Colonius, 2019) to capture both short and long wave range interactions and can be

considered as two-way coupled model, where bubbles can directly feel the acoustic field emitted by each other. An intrinsic difficulty in these models is how to account for the influence of the liquid compressibility on the multiple interactions among bubbles. Indeed one of the most frequently-used assumption is to resort to the incompressible limit, where we neglects any time-delay effect due to liquid compressibility and the interactions among bubbles take place instantaneously . Although this assumption is certainly valid when the wavelength of the excitation pressure wave is much larger than the characteristic size of the bubble cluster, the accuracy of applicability of these models in systems with many bubbles has not been discussed in detail.

Some numerical studies applied to medical related research such as high-intensity focused ultrasound (Okita *et al.*, 2013), ultrasound contrast agent (Faez *et al.*, 2012), and drug delivery (Coussios and Roy, 2008) point out the importance of compressibility effects, in particular time-delay effects in real applications (Sujarittam and Choi, 2020). More fundamental studies including experimental works studying the acoustic propagation in the vicinity of a bubble chain (Manasseh *et al.*, 2004) have shown that the time-delay effects considerably change the resonance frequencies and the damping factors of the effective medium (Doinikov *et al.*, 2005; Ooi *et al.*, 2008), so does bubble near boundaries (Dahl and Kapodistrias, 2003; van't Wout and Feuillade, 2021; Ye and Feuillade, 1997). In the context of the development of acoustic metamaterials, two-dimensional bubble layers also known as bubbly screens have also became a widely investigated system since 2009 in a series of papers published by Leroy and coworkers (Leroy *et al.*, 2015, 2009; Lombard *et al.*, 2015).

Using the self-consistent approach based on the effective medium theory, the transmission and reflection coefficient measured experimentally in the linear regime can be well captured by accounting for the influence of time-delay effects on the interaction term among bubbles. In the non-linear regime, the asymptotic analysis based on effective medium theory (Miksis and Ting, 1989; Pham *et al.*, 2021) have shed light into the role of compressibility on the mechanisms of multiple interactions among bubbles. However, these models still face some challenges. For example, it is known that, even in the dilute limit, crystal configuration has special acoustic properties (Devaud *et al.*, 2010), but the capability of effective medium theory to distinguish between the properties of specific configurations (e.g. crystals) and the ensemble average of randomly distributed systems has not been clarified . Also, it is not clear how well averaged models capture the influence of boundary effects as well as polydispersity effects.

In this work we discuss the applicability and the accuracy of models based on a coupled system of RP like equations to capture the response of bubbly screens (Figure 1). Section II presents a particularization of the system of Rayleigh-Plesset like equations proposed in Fuster and Colonius (2011) to solve for the dynamic response of the bubbles. In SectionIII , we show that, without the need of introducing any fitting parameter, this model is able to recover the second order solution predicted by the effective medium theory in the linear oscillating regime for a monodisperse bubbly screen in crystal configuration when the acoustic excitation wavelength is much larger than both the bubble radius and the inter-bubble distance. Then, we discuss the influence of boundary effects and randomness on the accu-

racy of the predictions in comparison with the effective medium theory in the linear regime. Finally, in Section IV, we present numerical results obtained in the non-linear regime using a delay differential equation solver. These examples reveal the importance of compressibility effects to correctly predict the non-linear bubble dynamic response.

II. BUBBLY SCREEN MODEL

The dynamics of an oscillating spherical bubble is described using the Keller-Miksis like equation (Keller and Miksis, 1980) which is a differential equation for the bubble radius of the ith bubble in a weakly compressible liquid characterized by its speed of sound c and density ρ

$$\rho\left(R_i\ddot{R}_i\left(1-\frac{\dot{R}_i}{c}\right)+\frac{3\dot{R}_i^{\,2}}{2}\left(1-\frac{\dot{R}_i}{3c}\right)\right)-\left(1+\frac{\dot{R}_i}{c}+\frac{R_i}{c}\frac{d}{dt}\right)(p_{i,B}-p_\infty)=\rho I_i. \quad (1)$$

In the equation above, $p_\infty(t)=p_0+f(t)$ is the pressure excitation; $p_{i,B}$ is the liquid pressure at the interface of the ith bubble, which we describe using a simple polytropic law $p_{i,B}=\left(p_0+\frac{2\sigma}{R_{i,0}}\right)\left(\frac{R_{i,0}}{R_i}\right)^{3\kappa}-\frac{2\sigma}{R_i}-\frac{4\mu\dot{R}_i}{R_i}$, where κ is the polytropic index; p_0 is the static pressure; $R_{i,0}$ is the ith bubble radius at equilibrium; σ is the surface tension; μ is the liquid viscosity. The interaction term ρI_i represents the pressure fluctuation induced by the presence of the surrounding bubbles, which has to be evaluated at the deferred time $t_{d_{ij}}=t-d_{ij}/c$, where $d_{ij}=|\vec{x}_i-\vec{x}_j|$ represents the distance from the ith bubble located at $\vec{x}_i$ to the jth bubble located at $\vec{x}_j$. Following Fuster and Colonius (2011), it can be readily shown that

$$I_i=I_{i,0}+I_{i,1}, \quad (2)$$

where both terms have to be evaluated at the deferred time $t_{d_{ij}}$

$$I_{i,0} = -\sum_{j\neq i}^{N} \frac{R_j(t_{d_{ij}})}{d_{ij}} \left(R_j(t_{d_{ij}})\ddot{R}_j(t_{d_{ij}}) + 2\dot{R}_j(t_{d_{ij}})^2 \right),$$

$$I_{i,1} = -\frac{1}{c}\left[\sum_{j\neq i}^{N} \frac{R_j(t_{d_{ij}})}{d_{ij}} \dot{R}_j(t_{d_{ij}}) \left[R_j(t_{d_{ij}})\ddot{R}_j(t_{d_{ij}}) + \frac{\dot{R}_j(t_{d_{ij}})^2}{2} - \frac{\left(p_{j,B}(t_{d_{ij}}) - p_\infty(t_{d_{ij}})\right)}{\rho} \right] \right.$$
$$\left. - \sum_{j\neq i}^{N} \frac{R_j(t_{d_{ij}})^2}{d_{ij}} \frac{d}{dt} \frac{\left(p_{j,B}(t_{d_{ij}}) - p_\infty(t_{d_{ij}})\right)}{\rho} + \dot{R}_i(t_{d_{ij}}) I_{i,0} \right]. \quad (3)$$

In the equations above, we only keep first order compressibility correction terms in the intensity of the collapse of bubbles, which scale as a function of the Mach number $Ma = \frac{\dot{R}}{c}$, and time-delay effects. Neglecting time-delay effects (e.g. $t_{d_{ij}} = t$) leads to a coupled system of ordinary differential equations that need to be solved. In the limit of $c \to \infty$, we recover the classical form of the interaction term $I_i \approx I_{i,0}$ evaluated at t (Bremond *et al.*, 2006; Ida *et al.*, 2007; Yasui *et al.*, 2008). Otherwise, as explained in Section IV, it is required to solve a differential equation with time delays.

For monodisperse bubbles, where $R_{i,0} = R_{j,0} = R_0$, the development of liquid compressibility corrections is typically discussed in terms of the nondimensional wavenumber kR_0, where $k = \omega/c$. For air/water systems at constant reference pressure, $kR_0 = \frac{\omega}{\omega_0}\frac{1}{c}\sqrt{\frac{3\kappa p_0}{\rho}}$ depends on the frequency ratio between the excitation frequency, ω, and the resonance frequency of single isolated oscillating bubble, $\omega_0 = \sqrt{\frac{3\kappa p_0}{R_0^2\rho}}$. For air bubbles in water at atmospheric conditions, $\frac{1}{c}\sqrt{\frac{3\kappa p_0}{\rho}} \approx 10^{-2}$ (this parameter will be held constant in the following solution for particular configurations of the bubbly screen), and, therefore, kR_0 is small except for very high frequencies. However, in addition to kR_0, it is useful to introduce an alternative dimensionless wavenumber using the inter-bubble distance D ($kD = \frac{D}{R_0}\frac{\omega}{\omega_0}\frac{1}{c}\sqrt{\frac{3\kappa p_0}{\rho}}$)

which is not always small in diluted systems. kD, kR_0 and $\frac{D}{R_0}$ construct the ratio of the three relevant spatial scales (the wavelength, the inter-bubble distance, and the bubble equilibrium radius) considered in this work to characterize the bubble screen.

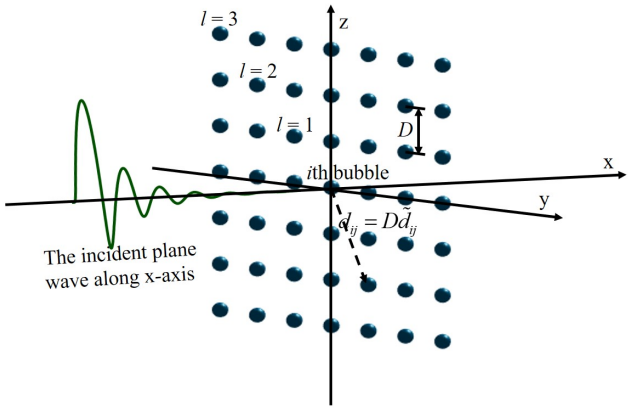

FIG. 1. A typical crystal distributed bubbly screen located at $x = 0$ plane.

The particular arrangement of bubbles considered in this work is that of a finite/infinite bubbly screen (Figure 1) in which bubbles are located in the $x = 0$ plane, perpendicular to the incident wave, in layers around a central bubble. Any bubble under consideration will always be labelled with subscript i. In the lth layer, bubbles are equally spaced with a given inter-bubble distance D along a square of size $2lD$ centered at the bubble under consideration. The position and the dispersity of the bubbles will be eventually perturbed when discussing randomization effects in the linear regime.

III. COMPRESSIBILITY EFFECTS IN THE LINEAR OSCILLATION REGIME

A. General case

We start considering the dynamics of a finite bubbly screen with monodisperse bubbles excited by a weak perturbation, where $R_{i,0} = R_{j,0} = R_0$. For a system with N bubbles, Eq. 1 reduces to

$$R_i\ddot{R}_i - \left(1 + \frac{R_i}{c}\frac{d}{dt}\right)\frac{p_{i,B} - p_\infty}{\rho} = -\sum_{j\neq i}^{N}\frac{R_j^2(t_{d_{ij}})}{d_{ij}}\ddot{R}_j(t_{d_{ij}}) + \sum_{j\neq i}^{N}\frac{R_j(t_{d_{ij}})}{d_{ij}}\frac{R_j(t_{d_{ij}})}{c}\frac{d}{dt}\frac{\left(p_{j,B}(t_{d_{ij}}) - p_\infty(t_{d_{ij}})\right)}{\rho}. \tag{4}$$

Note that in the linear regime, the influence of the compressibility correction term in the interaction is not null, and it is not sufficient to retain the classical interaction term $I_{i,0}$ only.

For a general case where the pressure at the location of the ith bubble is presented as $p_\infty(\mathbf{x}_i, t) = p_0(1 + p_i' e^{\imath\omega t})$, the solution of the equation for the ith bubble can be expressed in the form of $R_i(t) = R_0(1 + r_i' e^{\imath\omega t})$. Taking $R_j(t_{d_{ij}}) = R_0(1 + r_j' e^{\imath\omega(t - d_{ij}/c)})$, the values of r_i' are obtained from the solution of a linear system, which in indicial notation can be written as

$$\left(A_{ij}^{(0)} + \imath k R_0 A_{ij}^{(1)}\right) r_j' = -\frac{p_0}{\rho R_0^2 \omega_0^2} p_i'. \tag{5}$$

The coefficients of the matrices $\mathbf{A}^{(0)}$ and $\mathbf{A}^{(1)}$ are given in Appendix A neglecting viscous, thermal, mass transfer and surface tension terms as well as terms of order $(kR_0)^2$ during linear analysis. The first choice is justified by the fact that the influence of interactions on the bubble dynamics can be discussed as a correction of the resonance frequency and the radiative damping introduced by compressibility effects (Leroy *et al.*, 2009; Pham *et al.*, 2021). For a particular application, it would be straightforward to extrapolate the results

to situations where the influence of the effects neglected are relevant using corrected linear expressions to express the bubble pressure (Bergamasco , 2017; Fuster and Montel, 2015). Neglecting $(kR_0)^2$ terms is justified by the fact that $kR_0 \approx 10^{-2}\frac{\omega}{\omega_0}$ is usually small, and ignoring higher order terms is a valid assumption except for extremely high frequencies. In this simplified case, matrices $\mathbf{A}^{(0)}$ and $\mathbf{A}^{(1)}$ only depend on the local variable $\mathfrak{K}_i = \frac{R_0}{D}\sum_{j\neq i}^{N}\frac{e^{-\imath kD\tilde{d}_{ij}}}{\tilde{d}_{ij}}$, which represents the strength of the interaction term and depend on the nondimensional distance $\tilde{d}_{ij} = |\vec{x}_i - \vec{x}_j|/D$.

For a planar wave, the linear set of equations in Eq. 5 can be numerically solved for an arbitrary constant value of $p'_i = p'_j = p'$ for all bubbles to find all r'_i. Once these values are obtained, we can re-express any equation in the system as

$$\left(-\omega^2 - K_i^*\omega^2 + \omega_0^2\right) r'_i = -\frac{p_0}{\rho R_0^2}p', \tag{6}$$

where, for any arbitrary ith bubble under consideration, we have

$$K_i^* = \mathfrak{K}_i(1 - Q_i^*) - \imath kR_0\left[(1+\mathfrak{K}_i)^2 - \mathfrak{K}_i Q_i^*\left(1 + \mathfrak{K}_i + \frac{\omega_0^2}{\omega^2}\right)\right], \tag{7a}$$

$$Q_i^* = \frac{\sum_{j\neq i}^{N}(r'_i - r'_j)\frac{e^{-\imath kD\tilde{d}_{ij}}}{\tilde{d}_{ij}}}{r'_i\sum_{j\neq i}^{N}\frac{e^{-\imath kD\tilde{d}_{ij}}}{\tilde{d}_{ij}}}. \tag{7b}$$

Equation 6 is similar to the harmonic form of single bubble situation

$$(-\omega^2 + \imath\zeta_i\omega^2 + \omega_{i,res}^2)r'_i = -\frac{p_0}{\rho R_0^2}p', \tag{8}$$

where the local bubble resonance frequency and the local damping factors can be readily obtained as

$$\omega_{i,res}^2 = \omega_0^2\left(1 - \Re(K_i^*)\left(\frac{\omega}{\omega_0}\right)^2\right);\ \zeta_i = -\Im(K_i^*). \tag{9}$$

Function K_i^* gathers both interaction and compressibility effects in the bubble resonance and the damping of the bubble and depends on the quantity Q_i^* which provides a measure of the correlation between the radial bubble motion of the ith bubble and that of the surrounding bubbles. Q_i^* becomes zero in the limiting case of synchronous motion. It is also easy to verify that in the limit of an isolated bubble, $\mathfrak{K}_i \to 0$, we recover the well known result, $\omega_{i,res}^2 = \omega_0^2$ and $\zeta_i = \zeta = kR_0$, representing the harmonic oscillation of a single bubble in a slightly compressible liquid. For systems where K_i^* is not uniform for all the bubbles, multiple local resonances appear.

To characterize the global response of the screen, it is useful to express the averaged gas volume evolution as a function of the amplitude of the driving pressure

$$\left(-\omega^2 + \imath\zeta\omega^2 + \omega_{res}^2\right) \frac{1}{N} \sum_{i=1}^{N} r_i' = -\frac{p_0}{\rho R_0^2} p'. \tag{10}$$

Using Eq. 6, the global resonance and damping factor can be readily found as a function of the complex averaged function K^* as

$$\omega_{res}^2 = \omega_0^2 \left(1 - \Re(K^*)\frac{\omega^2}{\omega_0^2}\right);\ \zeta = -\Im(K^*);\ K^* = \frac{\langle K_i^* r_i' \rangle}{\langle r_i' \rangle}. \tag{11}$$

where the symbol $\langle \cdot \rangle$ denotes the average over all the bubbles in the screen.

B. Synchronous solution for an infinite bubbly screen with crystal configuration

We start considering the synchronous solution for an infinite bubbly screen with equal amplitude for the radial motion of all bubbles. In this limit, $r_i' = r_j' = r'$, $\mathfrak{K}_i = \mathfrak{K}_j = \mathfrak{K}$,

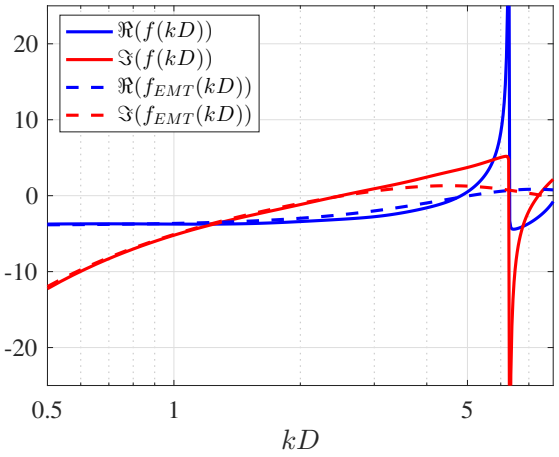

FIG. 2. Real and imaginary part of the function $f(kD)$. For reference we include the predictions of the effective medium theory. The solid line is corresponding to the $f(kD)$ and the dashed line is corresponding to EMT. The blue line is the real part, and the red line is the imaginary part. $N_l = 12000$ is used to keep $f(kD)$ converge.

$Q_i^* = 0$, and the solution of the system is thus given by the simplified expression

$$K_i^* = K^* = \mathfrak{K} - \imath k R_0 (1 + \mathfrak{K})^2, \tag{12}$$

where $\mathfrak{K} = \frac{R_0}{D} f(kD)$ is a function that is proportional to the bubble inter-spacing parameter R_0/D and function

$$f(kD) = \sum_{j \neq i}^{\infty} \frac{e^{-\imath k D \tilde{d}_{ij}}}{\tilde{d}_{ij}} \tag{13}$$

depends on the dimensionless wavenumber kD and the particular geometry considered only. Notice that, so far, the subscript i is still hold here to represent the bubble inside the infinite bubbly screen under consideration, but that $f(kD)$ doesn't change with respect to the choice of the bubble i. Taking advantage of rotation invariance of the system, the value of this function can be obtained from a double sum over the layers surrounding an arbitrary bubble

as

$$f(kD) = \sum_{l=1}^{\infty} \frac{4}{l} e^{-\imath kDl} \left(1 + \sum_{q=1}^{l} \frac{2}{\sqrt{1+(q/l)^2}} e^{\imath kDl\left(1-\sqrt{1+(q/l)^2}\right)} \right). \tag{14}$$

Eq. 14 can be evaluated numerically except in very particular cases. For instance, if $kD = 2\pi n$ with n being an integer, the first term will be a diverging harmonic series implying zero resonance frequency and infinite attenuation.We identify this phenomenon with a resonance phenomenon in the spacing within the bubbles. The convergence properties of this series in a general case are discussed in Appendix B. It is interesting to note that the results obtained are in agreement with the expression proposed by Leroy *et al.* (2009) who, taking advantage of an homogeneization approach and introducing a cuttoff length $b = D/\sqrt{\pi}$, obtain $\mathfrak{K}$ using the bubble density $n_d = 1/D^2$ (number of bubbles per unit area in the screen) as

$$\mathfrak{K}_{\mathrm{EMT}} = \frac{R_0}{D} f_{\mathrm{EMT}}(kD) \approx \int_b^{\infty} \frac{R_0}{r} e^{-\imath kr} 2\pi r n_d dr = \frac{R_0}{D} f_{\mathrm{EMT}}(kD), \tag{15}$$

$$f_{\mathrm{EMT}}(kD) = -\frac{2\pi}{kD} \left(\sin(kb) + \imath \cos(kb) \right). \tag{16}$$

As shown by Pham *et al.* (2021), this expression is similar to the extension of the asymptotic analyses proposed by Caflisch *et al.* (1985) and later extended by Miksis and Ting (1989) to the second order, where the correction due to the collective effects of the bubbly screen is (Pham *et al.*, 2021)

$$f_{\mathrm{EMT}}(kD) = -3.9 - \imath \frac{2\pi}{kD}. \tag{17}$$

Using the small angle approximation, it is straightforward to see that Eqs. 17 and 16 are equivalent and, as shown in Figure 2, reproduce well the values of the series for $kD \lesssim 3$ without the need of introducing any fitting parameter. In what follows we denote the predictions of this model as effective medium theory (EMT). Note that although the function

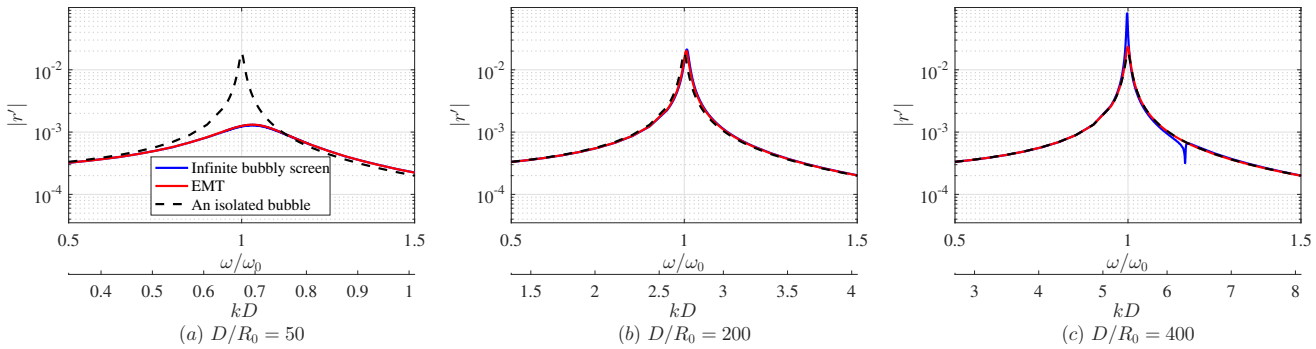

FIG. 3. Non-dimensional amplitude of the bubble oscillation in an infinite bubbly screen $|r'|$ as a function of ω/ω_0 for three different concentrations. The series are evaluated using $N_l = 12000$ layers. The curves predicted by EMT and the current model fit well with each other when $\frac{D}{R_0} = 50$ and gradually trend to the isolated bubble situation when $\frac{D}{R_0} = 200$. For $\frac{D}{R_0} = 400$, EMT recovers the solution of the single bubble case missing the resonance phenomenon captured by the current model.

$f(kD)$ is correctly predicted, EMT still neglect the correction of order $(kR_0 \cdot \mathfrak{K})$ in the bubble dynamic motion.

Figure 3 represents the nondimensional amplitude of the bubble oscillation $|r'|$ as a function of the frequency for three different concentrations for $\frac{p_0}{\rho R_0^2 \omega_0^2} = 0.25$ and $|p'| = 10^{-3} p_0$. For high concentrations $(D/R_0 = 50)$ the resonance peak is damped, this effect being well captured by the EMT. As the bubble concentration is decreased, EMT recovers the solution of the single bubble case missing the resonance phenomenon captured by the current model. Remarkably, the intensity of the peak at resonance becomes much more important than the one predicted by the EMT with the increasing of kD. To gain further insight, Figure 4 shows

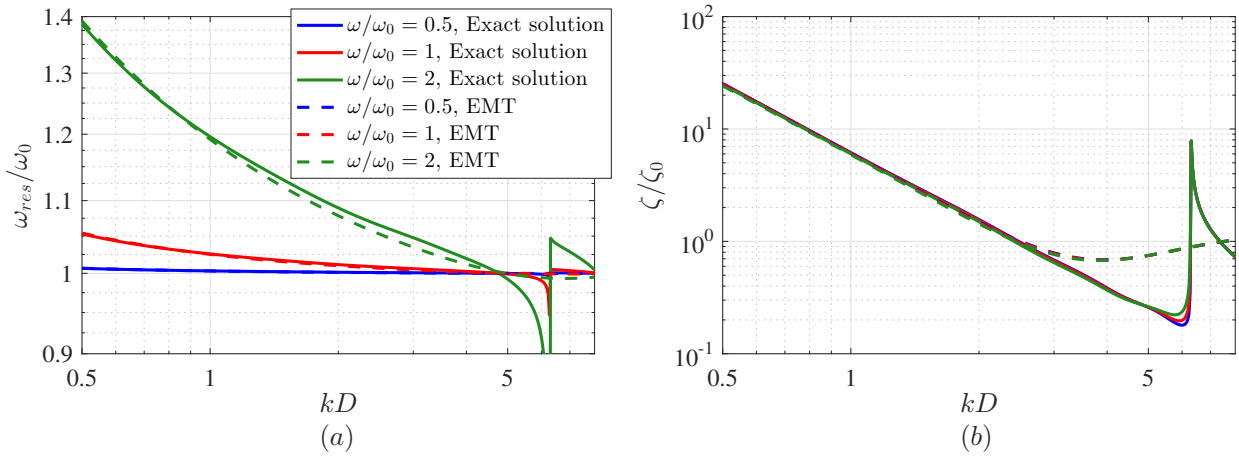

FIG. 4. (Left) Concentration effects on ω_{res}/ω_0 and (right) on ζ/ζ_0. Solid lines are used for the approximated exact solution ($N_l = 12000$). Dashed lines represent the solution provided by the effective medium theory. The frequencies used are $\omega/\omega_0 = 0.5, 1, 2$ for blue, red and green line respectively.

the influence of D/R_0 at constant forcing frequency on the global resonance and the global damping factor. By changing the inter-bubble distance, the proposed model recovers well the predictions of the effective medium approximation for $kD \lesssim 3$, while for large values of kD both models give different predictions. This discrepancy is attributed to the difference between crystal structure and the random bubble distribution as discussed later on for a finite bubbly screen. In the effective medium approximation, bubbles are continuously and homogeneously distributed in the space, and the oscillating term $e^{-ikD\tilde{d}_{ij}}$ is thus smoothed out. The current model is able to capture the resonance effects originated for particular configurations. In the particular example shown here, it is expected to find a first resonance for $kD = 2\pi$, corresponding to the appearance of the resonance induced by the inter-bubble

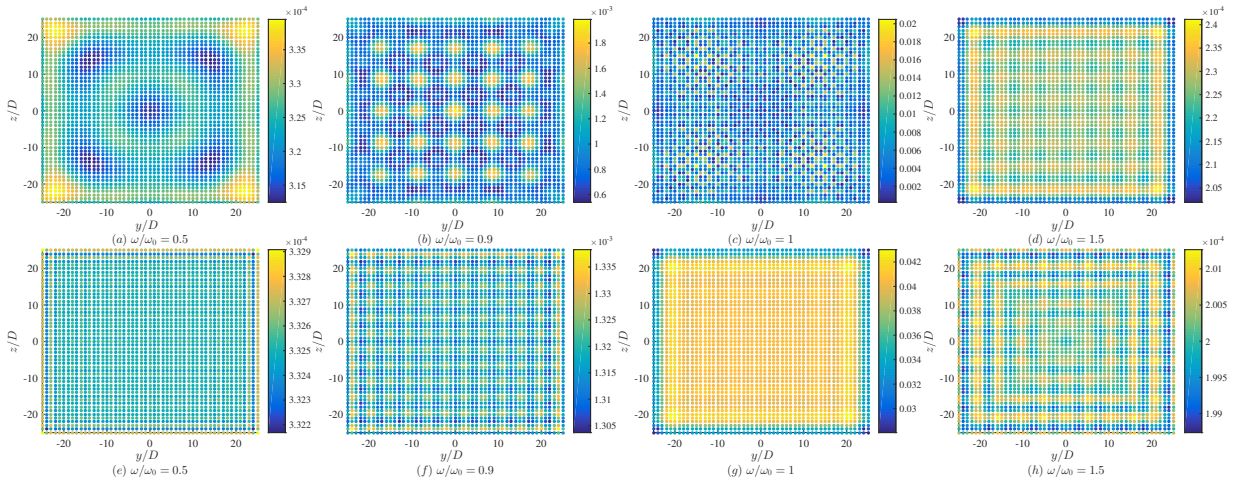

FIG. 5. Distribution of the amplitude of the nondimensional bubble oscillation $|r'|$ for different values of ω/ω_0 in a 51×51 bubbly screen for (top) $D/R_0 = 50$ ($kD = 0.67$) and (bottom) $D/R_0 = 400$ ($kD = 5.4$).

distance.

C. Finite size bubbly screens

In many applications, the size of the bubbly screens is limited to few tens or hundreds of bubbles, and the infinite screen limit may not be applicable. Figure 5 shows examples of the distribution of the nondimensional bubble oscillation amplitude $|r_i'|$ for a 51×51 bubbly screen excited at the single bubble resonance frequency for two different values of the dimensionless wavenumber: $kD = 0.67 < 1$ and $kD = 5.4$. Characteristic spatial patterns are easily identified at resonance conditions but also become visible for other specific values of the forcing frequency. This phenomenon is related to the appearance of multiple resonance

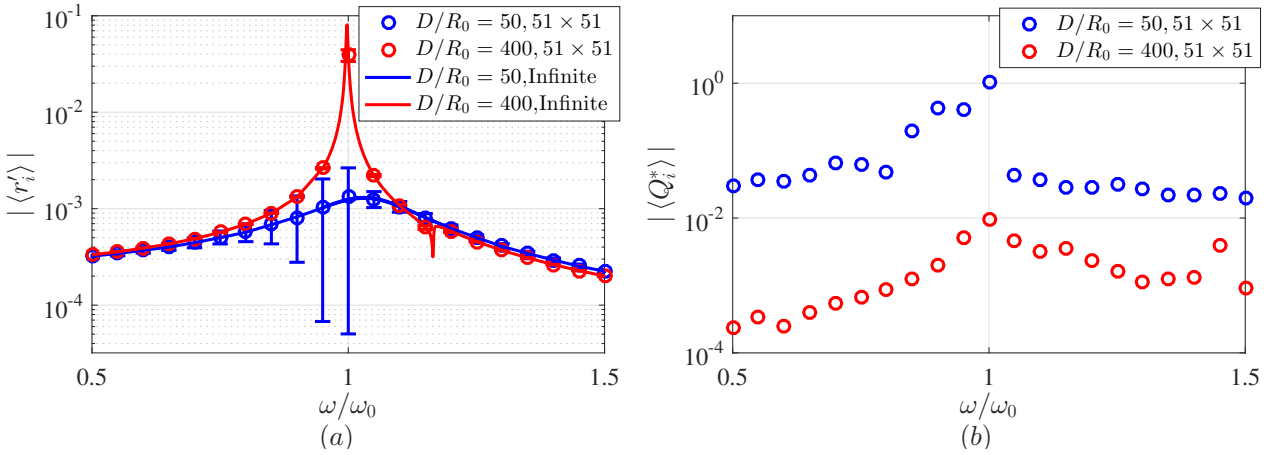

FIG. 6. (a) Averaged amplitude of the bubble oscillation $|\langle r_i' \rangle|$ (errorbar represents the standard deviation of $|\langle r_i' \rangle|$) and (b) $|\langle Q_i^* \rangle|$ of a 51×51 bubbly screen as a function of frequency.

frequencies in the system. Figure 6a shows that, as in the infinite case, the intensity of the mean value of r_i' becomes maximum at resonance, fitting the infinite bubbly screen well. The distribution of local resonance frequencies is represented using the intensity of the standard deviation of r_i' (errorbars in Figure 6a) and the averaged value of Q_i^* (Figure 6b) which tends to a plateau at larger frequencies and quickly decays for low frequencies.

The role of the concentration on $|\langle Q_i^* \rangle|$ is shown in Figure 7. At resonance (Figure 7b), we observe a sharp transition between $kD \leq 2$, where the fluctuations of $|\langle Q_i^* \rangle|$ become of order unity, and $kD > 2$, where $|\langle Q_i^* \rangle|$ takes significantly smaller values. Remarkably, in the regime of $kD \leq 2$, we do not see any clear asymptotic convergence to $|\langle Q_i^* \rangle| \to 0$ as we increase the number of bubbles in the screen. Below resonance (Figure 7a), the value of $|\langle Q_i^* \rangle|$ is small and slow convergence to zero is observed for the screens considered. One of the reasons for the slow convergence may be the excitation of non-uniform modes induced by boundary effects. The consequences of perturbation on the plane containing the bubbles

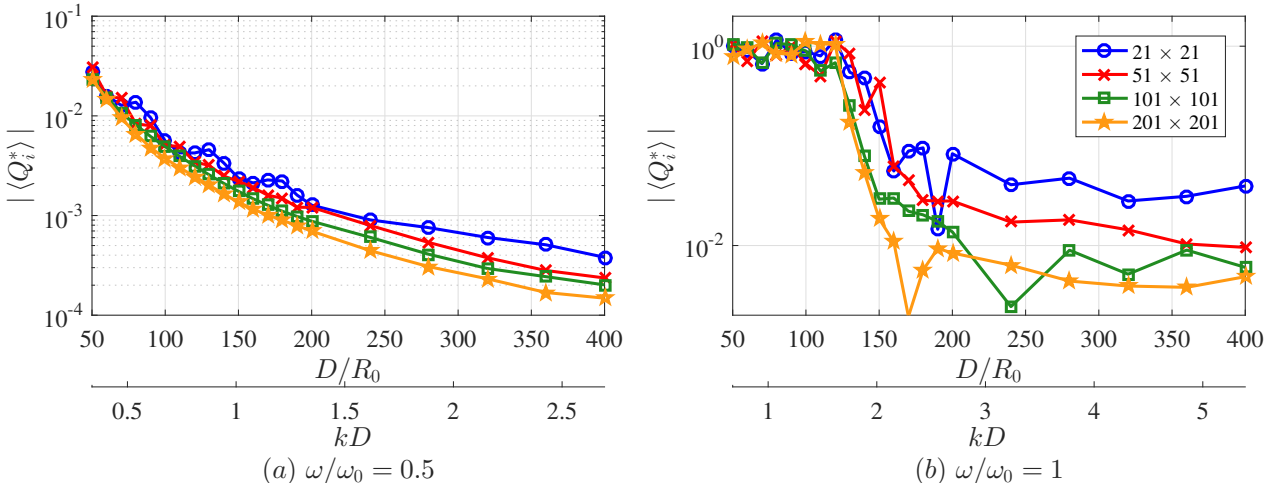

FIG. 7. Influence of concentration on $|\langle Q_i^* \rangle|$ for various finite size bubbly screens and two different values of ω/ω_0.

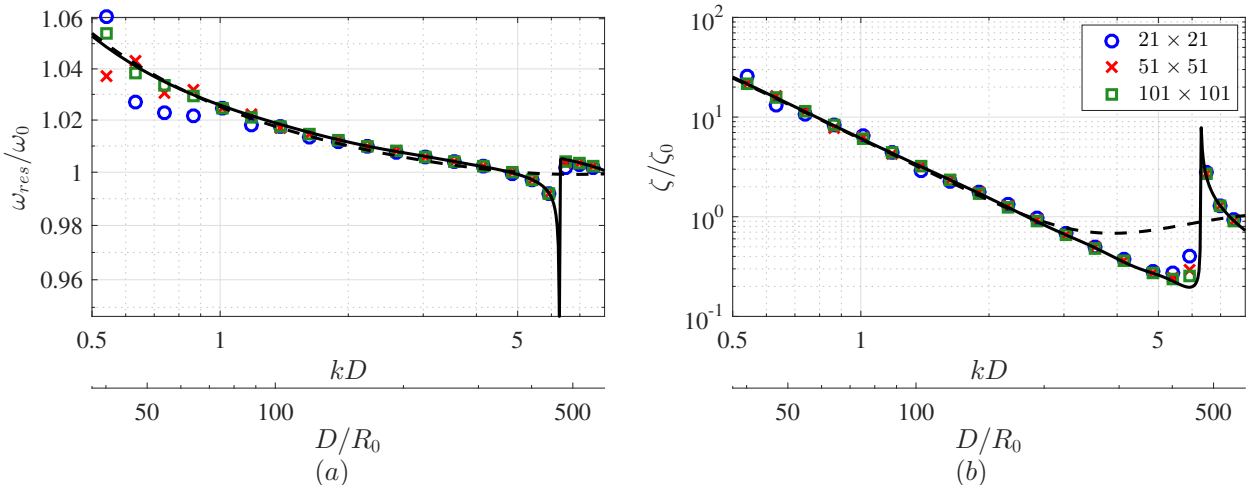

FIG. 8. Global resonance frequency and the global acoustical damping factor of finite bubbly screen with different screen sizes for $\omega/\omega_0 = 1$. 21×21 (blue circle), 51×51 (red cross sign) and 101×101 (green square). The theoretical curves calculated for an infinite system (black solid line, $N_l = 12000$) and effective medium theory are included for reference (dashed line).

in the infinite case (we have imposed an unperturbed planar wave in the y-z plane) is left for future works.

The effect of finite size effects on the global resonance frequency and the global damping factor can be seen in Figure 8 for $\omega/\omega_0 = 1$. The infinite bubbly screen limit captures accurately the averaged bubble response of the screen, only showing some small disagreement for very concentrated systems, where we have seen the non-uniformity on the bubble response is important.

D. Randomization

We further discuss the influence of the randomness on the position and on the polydispersity of the bubbles separately. To that end, we firstly perturb the position of each bubble by a random number $-\Theta_P < \theta_{y/z} < \Theta_P$ with respect to the crystal configuration so that ith bubble is located at $\vec{x}_i = (0, y_i^{(c)} + \theta_{y,i}D, z_i^{(c)} + \theta_{z,i}D)$, where the superscript $^{(c)}$ stands for variables corresponding to the crystal configuration. Figure 9(a,b) shows the global factors defined in Eq. 11 averaged over 100 realizations for $\omega/\omega_0 = 1$ using a finite screen with 51×51 bubbles with different Θ_P. As expected, the resonance effects observed at $kD = 2\pi$ quickly vanish as the randomization parameter increases. Remarkably, the results obtained differ from the effective medium theory for large values of the randomization parameter and intermediate values of kD, the effect of randomization being especially visible on the effective damping coefficient.

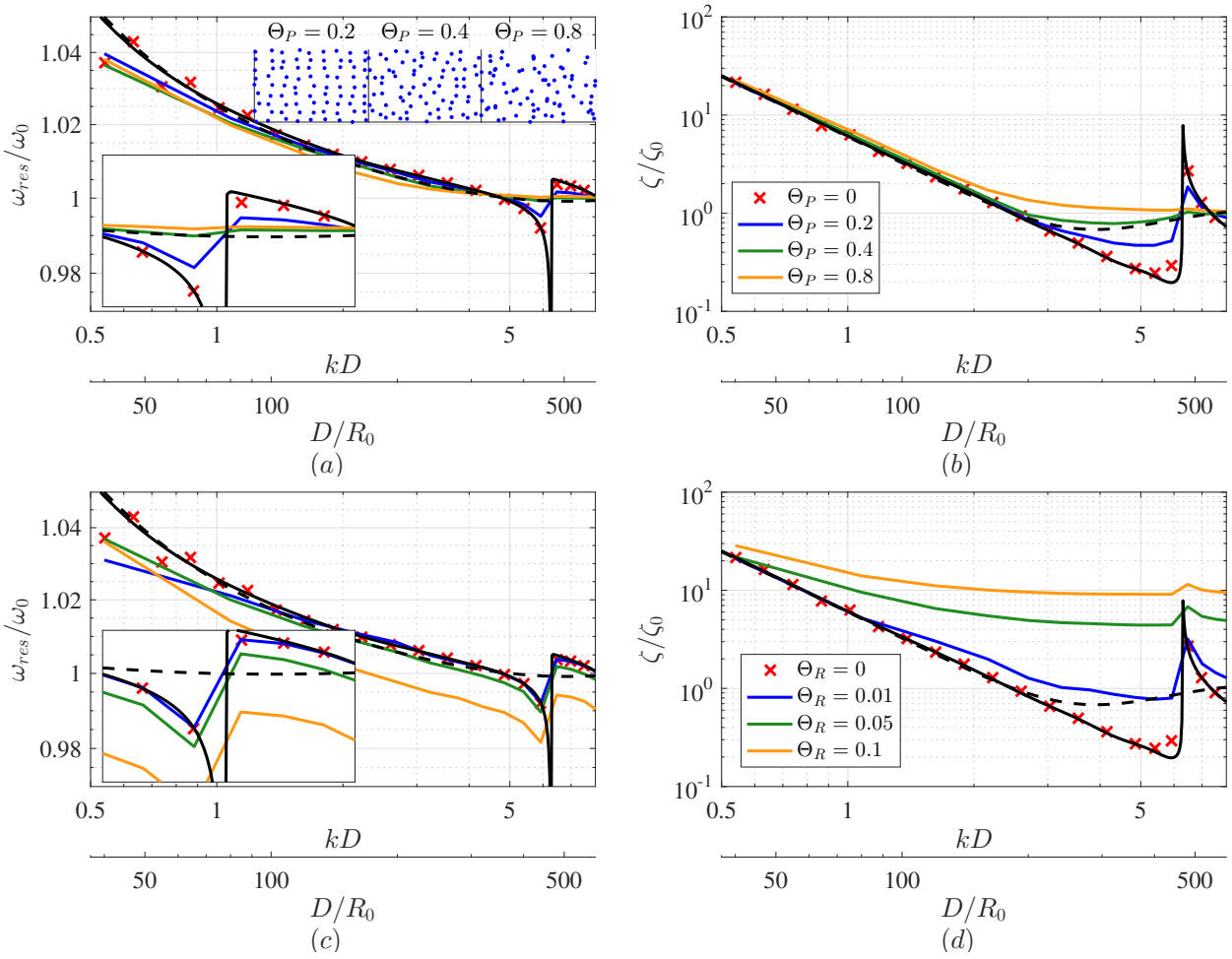

FIG. 9. Influence of (top) spatial randomness and (bottom) polydispersity for (left) the global resonance and (right) the global damping coefficient for a 51×51 finite bubbly screen using $\omega/\omega_0 = 1$. An example of the spatial distribution of the bubble positions is given in the inset of (a). For reference we include curves calculated for an infinite system (black solid line, $N_l = 12000$) and effective medium theory (dashed line).

In this case, both matrix $\mathbf{A}^{(0)}$ and $\mathbf{A}^{(1)}$ can be further decomposed as a globally uniform value given by the crystal structure and a correction directly attributed to randomization (see Appendix A). While the expectation of $\mathbf{A}'^{(0)}$ is zero, the non-linear term in the $\mathbf{A}'^{(1)}$ matrix with respect to the position perturbation amplitude makes the averaged response

of the system to be different from the crystal situation for small perturbations. For large perturbations, the expectation of both $\mathbf{A}'^{(0)}$ and $\mathbf{A}'^{(1)}$ are a-priori different from zero and depend on the value of Θ_P. In such a situation, the difference between the fluctuation around the crystal configuration and the completely random distribution also makes the averaged response of the system to be different from EMT. In Figures 9(a,b) we see that the randomization intensity parameter Θ_P mainly increases the effective damping for $kD > 1$.

The influence of polydispersity is depicted in Figure 9(c,d). The equilibrium bubble radius of each bubble is perturbed with a random number $-\Theta_R < \theta_R < \Theta_R$ with respect to R_0, such that $R_{i,0} = (1 + \theta_{R,i})R_0$. The same averaging process is repeated to obtain the global factors. As it occurs in the problem of linear wave propagation in bubbly liquids, the influence of polydispersity is mainly visible in the damping coefficients, playing a minor role on the shift of the resonance frequency. Notice that, different from the spatial randomness which is unavoidable restricted by the current technology, the polydisperse randomness plays a minor role in the experimental environments (Leroy *et al.*, 2009), and a detailed theoretical analysis is left for future publications.

IV. COMPRESSIBILITY EFFECTS IN THE NON-LINEAR REGIME

A. Numerical methods for differential equations with time delays

In the non-linear regime, it is no longer possible to find analytical solutions and one needs to solve the set of ODEs numerically. The differential equations considered can be written

as

$$\dot{y}(t) = f(t, y(t), y(t-\tau_1), ..., y(t-\tau_n), \dot{y}(t-\tau_1), ..., \dot{y}(t-\tau_n)), \tag{18}$$

where y is called state variable representing bubble radius or bubble wall velocity in our case. Traditionally, Eq. 18 is usually solved as ordinary differential equations, and the time-delay effect thus has to be ignored ($\tau_1, ..., \tau_n = 0$). In this work, when non-linear effects become important, Eq. 18 is directly solved, treated as neutral delay differential equation (NDDE), which will reduce to general delay differential equation (DDE) if $\dot{y}(t) = f(t, y(t), y(t-\tau_1), ..., y(t-\tau_n))$ and extend to state dependent NDDE if any of $(\tau_1, ..., \tau_n)$ is a function of state variable (Bellen and Zennaro, 2013). Integration of DDEs cannot be based on the mere adaption of some standard ODE code to the presence of delayed terms, which may dramatically modify the accuracy and stability of the underlying ODE method. To deal with NDDE, we first rewrite the Eq. 18 as:

$$\dot{y}(t) = f(y(t), y(t-\tau_1), ..., y(t-\tau_n), \frac{y(t-\tau_1) - y(t-\tau_1-\delta_t)}{\delta_t}, ..., \frac{y(t-\tau_n) - y(t-\tau_n-\delta_t)}{\delta_t}), \tag{19}$$

which is the dissipative approximation of the NDDE and named as retarded DDE. For small enough δ_t, the retarded DDE solver will be stable as long as the neutral DDE is stable. Based on Eq. 19, implicit Runge–Kutta formulas taking advantage of continuous extensions is used, and the retarded DDE is solved accordingly with residual control. The works of Shampine (2005, 2008) are recommended for detailed mathematical principles.

For simulations in temporal domain, delays needed to be considered should always be finite. Notice that, for any simulations with finite duration, e.g.,$[0, T]$, we only need to con-

sider the interactions from the bubbles with a distance from the bubble under consideration less than $d_{ij} <= cT$.

B. Numerical results

1. Weakly non-linear regime

One important aspect on the dynamic response of bubbly liquids is the appearance of subharmonics, which ultimately indicates the first transition route to the chaotic response obtained for large enough amplitude of excitation (Lauterborn and Cramer, 1981; Lauterborn and Koch, 1987). The harmonic components of the acoustic wave scattered by bubbles or ultrasound contrast agents are also important in medical applications (Halldorsdottir *et al.*, 2011; Nio *et al.*, 2019). The harmonics emitted by bubbles has been described by many authors (see Lauterborn and Kurz (2010) for a review), including studies for contrast agents in a free field (Andersen and Jensen, 2009; Katiyar and Sarkar, 2011). More recently Fan *et al.* (2020a) has revealed the impact of compressibility and bubble-wall interaction effects on the subharmonic emission of a bubble in a rigid tube. However, the influence of collective effects on the subharmonic emission has not been investigated in detail yet.

In this section, we compare the results obtained from the model presented for infinite bubbly screens imposing synchronous motion ($R_i = R_j = R$) with the results obtained from the EMT in non-linear regimes (Pham *et al.*, 2021) where

$$I_{EMT} = -2\pi c\dot{R}\frac{R^2}{D^2} + 3.9\frac{R}{D}(2\dot{R}^2 + \ddot{R}R). \tag{20}$$

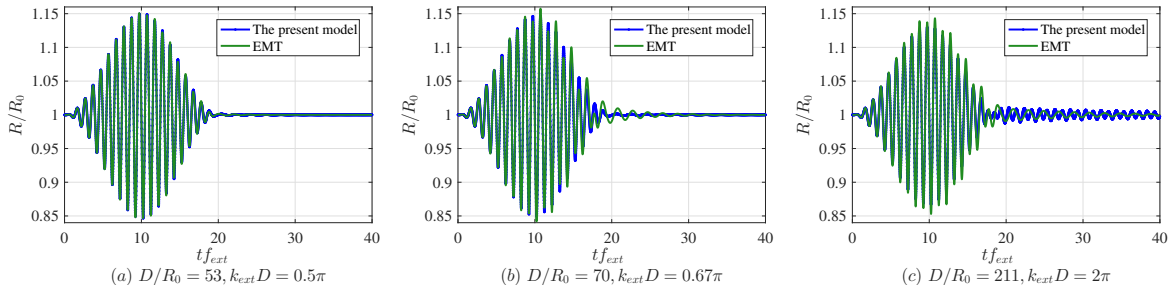

(a) $D/R_0 = 53, k_{ext}D = 0.5\pi$ (b) $D/R_0 = 70, k_{ext}D = 0.67\pi$ (c) $D/R_0 = 211, k_{ext}D = 2\pi$

FIG. 10. Influence of concentration on the radius v.s. time curves. $p_a = 2p_0 = 2bar$, $f_{ext} = 2f_0 = 1.409MHz$, and $R_0 = 5\mu m$.

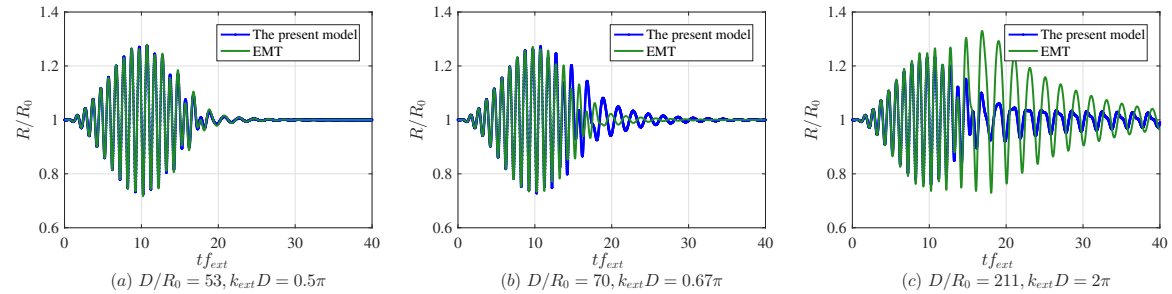

(a) $D/R_0 = 53, k_{ext}D = 0.5\pi$ (b) $D/R_0 = 70, k_{ext}D = 0.67\pi$ (c) $D/R_0 = 211, k_{ext}D = 2\pi$

FIG. 11. Influence of concentration on the radius v.s. time curves. $p_a = 3.5p_0 = 3.5bar$, $f_{ext} = 2f_0 = 1.409MHz$, and $R_0 = 5\mu m$.

To that end, we excite the bubbly screen with an incident pulse of the form

$$p_\infty(t) = p_0 - p_a \frac{1}{2}\left[1 - \cos\left(\frac{\omega_{ext}}{N_c}t\right)\right]\sin(\omega_{ext}t), \tag{21}$$

where $N_c = 20$, and $\omega_{ext} = 2\omega_0$ in order to favor the appearance of a stable subharmonic response. For simplicity, in this subsection we will only consider the response of an infinite bubble screen.

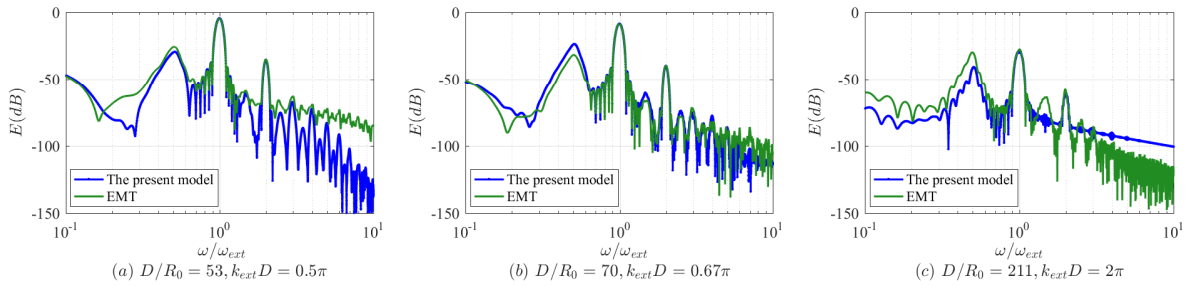

(a) $D/R_0 = 53, k_{ext}D = 0.5\pi$ (b) $D/R_0 = 70, k_{ext}D = 0.67\pi$ (c) $D/R_0 = 211, k_{ext}D = 2\pi$

FIG. 12. The frequency spectrum of the present model and EMT using $p_a/p_0 = 3.5$. The energy is calculated by $E = 20log_{10}(\frac{|\mathfrak{F}(p_{rad})|}{|\mathfrak{F}(p_{rad})_{max}|})$, where $|\mathfrak{F}(p_{rad})_{max}|$ is highest energy observed among all simulations.

In Figures 10-11, we can see the influence of concentration on the dynamic response of an infinite bubbly screen for two different excitation amplitudes. Consistent with the results in the linear regime, the effective medium model converges to the present model when the value of D/R_0, and therefore, $k_{ext}D$ is small. The differences between two models become significant with the increase of p_a/p_0 and $k_{ext}D$. Even in the case, where the differences between the two models are important (Figure 11c), both models fit relatively well for small times, and gradually become different only after some time. One explanation could be that in-phase and out-phase interactions coming from different layers at different time cancel each other and increase oscillatingly. Besides, the fact that the differences between models become visible after some time seem to indicate the differences of the EMT and the current model on the bifurcation diagrams (Lauterborn and Kurz, 2010).

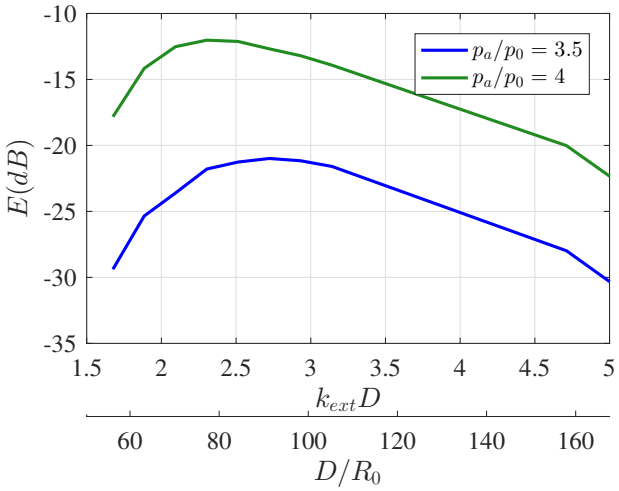

FIG. 13. Energy of the subharmonic emission as a function of concentration for a constant excitation frequency in a crystal structure.

Figure 12 shows the energy in the frequency spectrum of the infinite bubbly screen as a function of the bubble concentration from the radiated pressure (Pham *et al.*, 2021):

$$p_{rad} = 2\pi\rho c\frac{R^2\dot{R}}{D^2}. \tag{22}$$

The energy is calculated as $E = 20log_{10}(\frac{|\mathfrak{F}(p_{rad})|}{|\mathfrak{F}(p_{rad})_{max}|})$, where $\mathfrak{F}(\cdot)$ is the Fourier transform, and $|\mathfrak{F}(p_{rad})_{max}|$ is highest energy observed among all simulations. Because the frequency of the subharmonics slightly shifts from $\frac{\omega_{ext}}{2}$ with the increasing of the amplitude of the driving pressure wave, the corresponding energy is chosen according to the peak amplitude rather than energy at $\frac{\omega_{ext}}{2}$. As expected the energy on the fundamental component increases as D/R_0 decreases due to the increase of bubble concentration (Figure 12). The overall spectrum is well reproduced by the EMT except for $kD = 2\pi$, where we clearly see how the spectrum predicted by the EMT contains a significantly higher level of energy mainly concentrated at the subharmonics. In Figure 13, we show that optimal subharmonic emission

conditions appears for $k_{ext}D = [0.65, 0.75]\pi$ as a consequence of the crystal configuration. This effect is not captured by the EMT.

2. *Strongly non-linear regime*

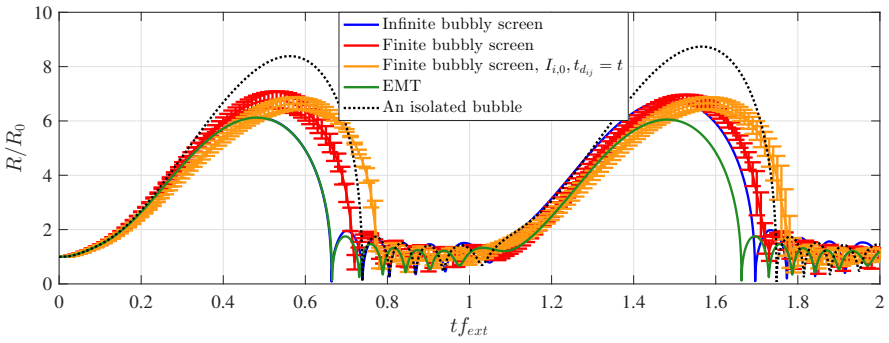

FIG. 14. Radius versus time curves predicted by different models for $D/R_0 = 134$ for an infinite bubbly screen oscillating synchronously and a 11×11 bubbly screen. $p_a = 2p_0 = 2bar$, $f_{ext} = 0.1f_0 = 70.461kHz$, and $R_0 = 5\mu m$. EMT and the infinite bubbly screen fit each other well up to the first rebound. In the later case, we show the averaged and the standard deviation of the bubble radius using the full model (red line) and the incompressible model wtih $I_i = I_{i,0}$ and $t_{d_{ij}} = t$ (yellow line).

When the excitation frequency is decreased ($\omega_{ext}/\omega_0 = 0.1$), the response of the bubbles become highly non-linear with a clear distinction between the expansion phase and the collapse and rebound region. In order to reduce the simulation time and transient effects, in this section we excite a bubbly screen with a perfect crystal configuration with an incident

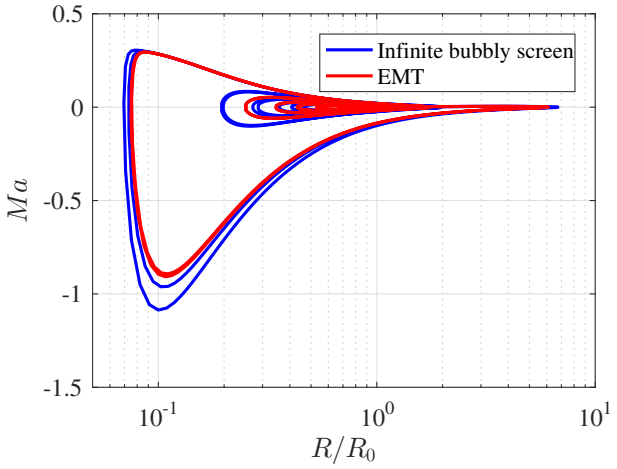

FIG. 15. Comparison of the trajectory of the averaged bubble radius versus $Ma = \dot{R}/c$ for the current model and the EMT.

planar wave represented by

$$p_\infty(t) = p_0 - p_a \sin(\omega_{ext} t).$$

The predictions of the temporal evolution of the bubble radius predicted by different models are given in Figure 14 for both infinite bubbly screens and finite bubbly screens. The amplitude of the initial expansion in all cases is decreased compared to the isolating oscillating bubble. The results from the EMT fit well the results of the infinite bubbly screen in the first expansion. The difference of the radial dynamics between different models appear in the rebound stage (Figure 15), when the Mach number($\dot{R}/c$) becomes important, so does the first order compressibility correction terms.

For completeness, in Figure 14 we also include the full simulation of a 11×11 bubbly screens. Because in this case bubble motion is no longer assumed to be synchronous, we

represent the averaged bubble radius among all bubbles in the screen as well as the standard deviation in one realization. The influence of the interactions on the finite screen is reduced in the expansion and is less strong comparing to the infinite case. Compressible effects play a visible role despite the long wavelength of the incident wave, and the classical incompressible bubble interaction model tends to over-predict the collapse time.

V. CONCLUSION

In this work, the compressibility effect on the bubble-bubble interaction is discussed. The model proposed in Fuster and Colonius (2011) is particularized to explicitely write a system of equations that account for first order correction compressibility effects. These effects are shown to be important compared with the classical incompressible interaction mechanism in Rayleigh–Plesset models.

In the linear regime, time-delay effects are always critical to capture the overall system response of large bubble screens. We show that the current model recovers the effective medium theory results up to second order for infinite crystal structures at large wavelengths ($kD \lesssim 3$). In addition, the model is able to capture resonant conditions in diluted systems due to crystal configurations that are not captured by averaged models. Randomization on the bubble position and boundary effects on bubbly screens of finite size are shown to be responsible to the appearance of characteristic periodic structures in the screen. These effects can modify the global damping measured under some conditions.

In the non-linear oscillating regime, we numerically solve the proposed model as a neutral delay differential set of equations (NDDE). The fully incompressible model seems to be only suitable to predict the expansion phase and loses its accuracy during the strong collapse where compressibility effects play a major role and need to be included. Boundary size effects are shown to limit the applicability of the effective medium theory valid only for infinite systems.

ACKNOWLEDGMENTS

This research has been supported by NSFC, Project No. U1809212, No. U1709203 and No. 41576102.

APPENDIX A:

When $p_i' \ll 1$, the system of Eq. 4 can be written in matrix form $\mathbf{A}\vec{r'} = -\frac{p_0}{\rho R_0^2 \omega_0^2}\vec{p'}$ with $\mathbf{A} = (\mathbf{A}^{(0)} + \imath k R_0 \mathbf{A}^{(1)})$, where

$$A_{ij}^{(0)} = \begin{cases} 1 - \left(\frac{\omega}{\omega_0}\right)^2 & \text{if } i = j, \\ -\left(\frac{\omega}{\omega_0}\right)^2 S_{ij} & i \neq j \end{cases}, A_{ij}^{(1)} = \begin{cases} \left(\frac{\omega}{\omega_0}\right)^2 (1 + \mathfrak{K}_i) - \mathfrak{K}_i & \text{if } i = j, \\ \left(\left(\frac{\omega}{\omega_0}\right)^2 (1 + \mathfrak{K}_i) + 1\right) S_{ij} & i \neq j \end{cases},$$

with $S_{ij} = \frac{R_0}{D} \frac{e^{-\imath k D \tilde{d}_{ij}}}{\tilde{d}_{ij}}$ and $\mathfrak{K}_i = \sum_{j \neq i}^{N} S_{ij}$.

In general cases using finite bubbly screen, bubbles may be not spatially arranged perfectly, and it is possible to rewrite this system by separating variables S_{ij} and $\mathfrak{K}_i$ into a crystal contribution and a spatially fluctuating part attributed to the perturbation of bub-

bles position

$$S_{ij} = S_{ij}^{(c)} + S'_{ij},$$

$$\mathfrak{K}_i = \mathfrak{K}_i^{(c)} + \mathfrak{K}'_i = \sum_{j\neq i}^{N} S_{ij}^{(c)} + \sum_{j\neq i}^{N} S'_{ij},$$

where the superscript $^{(c)}$ stands for variables corresponding to the crystal configuration, and the distances between bubbles is written as $\tilde{d}_{ij} = \tilde{d}_{ij}^{(c)} + \tilde{d}'_{ij}$. In this case, matrix $\mathbf{A}$ can be further decomposed as $\mathbf{A} \approx \mathbf{A}^{(C)} + \mathbf{A}'$ where $\mathbf{A}^{(C)}$ represents the value of $\mathbf{A}$ obtained with the values of a crystal structure and $\mathbf{A}'$ is the fluctuating part

$$A_{ij}^{\prime(0)} = \begin{cases} 0 & \text{if } i = j, \\ -\left(\frac{\omega}{\omega_0}\right)^2 S'_{ij} & \text{otherwise,} \end{cases}$$

$$A_{ij}^{\prime(1)} = \begin{cases} \left(\left(\frac{\omega}{\omega_0}\right)^2 - 1\right) \mathfrak{K}'_i & \text{if } i = j, \\ \left(\left(\frac{\omega}{\omega_0}\right)^2 + 1\right) S'_{ij} + \left(\frac{\omega}{\omega_0}\right)^2 (\mathfrak{K}'_i S'_{ij} + \mathfrak{K}_i^{(c)} S'_{ij} + \mathfrak{K}'_i S_{ij}^{(c)}) & \text{otherwise.} \end{cases}$$

When the position perturbation is small, taking advantage of Taylor expansion, we have:

$$S'_{ij} \approx -\imath k D \tilde{d}'_{ij} \frac{R_0}{D} \frac{e^{-\imath k D \tilde{d}_{ij}^{(c)}}}{\tilde{d}_{ij}^{(c)}}.$$

In such a situation, the expectation of $A_{ij}^{\prime(0)}$ is zero as long as the expectation of $\tilde{d}'_{ij}$ is zero. However the expectation of the $\mathfrak{K}'_i S'_{ij}$ term appearing in $A_{ij}^{\prime(1)}$, which acts like a variance term, is different from zero even for the small perturbations. Obviously when the amplitude of perturbation $\tilde{d}'_{ij}$ is large, the expectation of both $A_{ij}^{\prime(0)}$ and $A_{ij}^{\prime(1)}$ are a-priori different from zero.

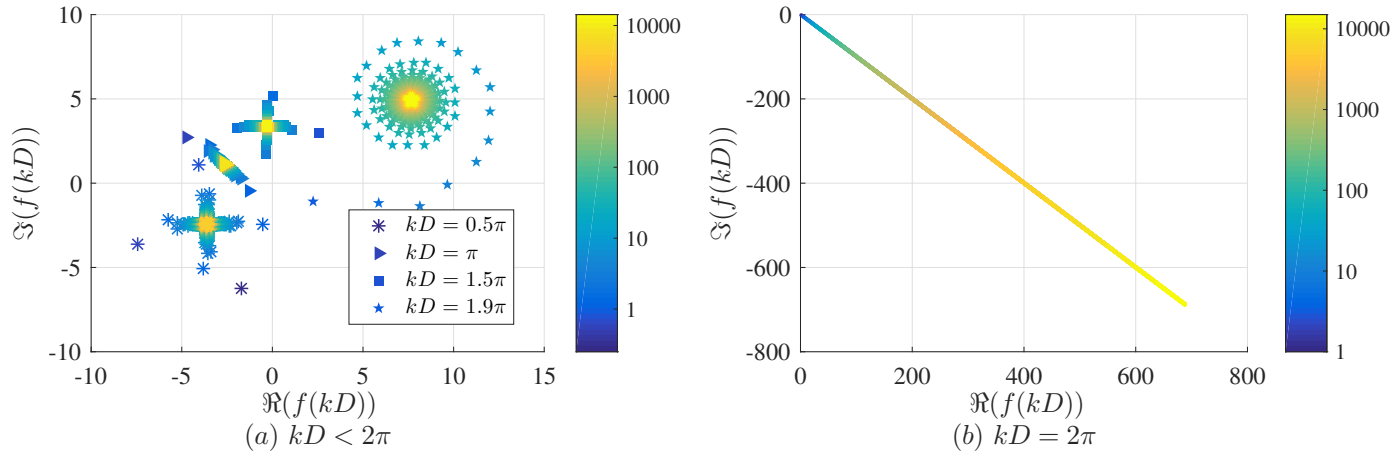

FIG. 16. Influence of the truncation N_l on the evaluation of the series in Eq. 14 for a crystal infinite screen and different values of kD. The colorbar represents the nondimensional truncation distance $N_l \frac{D}{\lambda}$.

APPENDIX B:

The convergence of the infinite series

$$f(kD) = \sum_{l=1}^{\infty} \frac{4}{l} e^{-\imath kDl} \left(1 + \sum_{q=1}^{l} \frac{2}{\sqrt{1+(q/l)^2}} e^{\imath kDl\left(1-\sqrt{1+(q/l)^2}\right)} \right)$$

is discussed as follows. For sufficiently large value of l, because quantity $p = \sqrt{1+(q/l)^2}$ is bounded between 1 and $\sqrt{2}$, we can approximate the series as

$$\sum_{q=1}^{l} \frac{2}{\sqrt{1+(q/l)^2}} e^{\imath kDl\left(1-\sqrt{1+(q/l)^2}\right)} \approx \int_1^{\sqrt{2}} \frac{2}{p} e^{\imath kDl(1-p)} dp = 2e^{\imath kDl} \left(E_{1/2}(\imath kDl) - 2^{1/4} E_{1/2}(\sqrt{2}\imath kDl) \right),$$

where $E(x)$ is the exponential integral function. Taking the limit for $l \to \infty$, we readily find that

$$\lim_{l\to\infty} \left(E_{1/2}(\imath kDl) - 2^{1/4} E_{1/2}(\sqrt{2}\imath kDl) \right) = 0$$

implying that this term always converges. The convergence of the series is then discussed in terms of the convergence of

$$\sum_{l=1}^{\infty} \frac{4}{l} e^{-\imath k D l} = \sum_{l}^{\infty} 4 \frac{z^l}{l} = 4 \ln\left(\frac{1}{1-z}\right)$$

where $z = e^{-\imath k D}$. For $kD = 2\pi n$ the series diverges and it converges otherwise. The influence of the number of layers considered on the series is reported in Figure 16 for different values of kD. In general, a very large value of the number of layers is required to accurately represent the infinity limit.

Andersen, K. S., and Jensen, J. A. (**2009**). "Ambient pressure sensitivity of microbubbles investigated through a parameter study," The Journal of the Acoustical Society of America **126**(6), 3350–3358.

Bellen, A., and Zennaro, M. (**2013**). *Numerical methods for delay differential equations* (Oxford university press).

Bergamasco, L., and Fuster, D. (**2017**). "Oscillation regimes of gas/vapor bubbles," International Journal of Heat and Mass Transfer **112**(), 72–80.

Bremond, N., Arora, M., Ohl, C.-D., and Lohse, D. (**2006**). "Controlled multibubble surface cavitation," Physical review letters **96**(22), 224501.

Caflisch, R. E., Miksis, M. J., Papanicolaou, G. C., and Ting, L. (**1985**). "Effective equations for wave propagation in bubbly liquids," Journal of Fluid Mechanics **153**, 259–273.

Commander, K. W., and Prosperetti, A. (**1989**). "Linear pressure waves in bubbly liquids: Comparison between theory and experiments," The Journal of the Acoustical Society of America **85**(2), 732–746.

Coussios, C. C., and Roy, R. A. (**2008**). "Applications of acoustics and cavitation to noninvasive therapy and drug delivery," Annu. Rev. Fluid Mech. **40**, 395–420.

Dahl, P. H., and Kapodistrias, G. (**2003**). "Scattering from a single bubble near a roughened air–water interface: Laboratory measurements and modeling," The Journal of the Acoustical Society of America **113**(1), 94–101.

Devaud, M., Hocquet, T., and Leroy, V. (**2010**). "Sound propagation in a monodisperse bubble cloud: From the crystal to the glass," The European Physical Journal E **32**(1), 13–23.

Doinikov, A. A., Manasseh, R., and Ooi, A. (**2005**). "Time delays in coupled multibubble systems (l)," The Journal of the Acoustical Society of America **117**(1), 47–50.

Faez, T., Emmer, M., Kooiman, K., Versluis, M., van der Steen, A. F., and de Jong, N. (**2012**). "20 years of ultrasound contrast agent modeling," IEEE transactions on ultrasonics, ferroelectrics, and frequency control **60**(1), 7–20.

Fan, Y., Li, H., and Fuster, D. (**2020**a). "Optimal subharmonic emission of stable bubble oscillations in a tube," Physical Review E **102**(1), 013105.

Fan, Y., Li, H., Zhu, J., and Du, W. (**2020**b). "A simple model of bubble cluster dynamics in an acoustic field," Ultrasonics sonochemistry **64**, 104790.

Foldy, L. L. (**1945**). "The multiple scattering of waves. i. general theory of isotropic scattering by randomly distributed scatterers," Physical review **67**(3-4), 107.

Fuster, D. (**2019**). "A review of models for bubble clusters in cavitating flows," Flow, Turbulence and Combustion **102**(3), 497–536.

Fuster, D., and Colonius, T. (**2011**). "Modelling bubble clusters in compressible liquids," Journal of Fluid Mechanics **688**, 352–389.

Fuster, D., and Montel, F. (**2015**). "Mass transfer effects on linear wave propagation in diluted bubbly liquids," Journal of Fluid Mechanics **779**, 598–621.

Gilmore, F. R. (**1952**). "The growth or collapse of a spherical bubble in a viscous compressible liquid," .

Halldorsdottir, V. G., Dave, J. K., Leodore, L. M., Eisenbrey, J. R., Park, S., Hall, A. L., Thomenius, K., and Forsberg, F. (**2011**). "Subharmonic contrast microbubble signals for noninvasive pressure estimation under static and dynamic flow conditions," Ultrasonic imaging **33**(3), 153–164.

Ida, M., Naoe, T., and Futakawa, M. (**2007**). "Suppression of cavitation inception by gas bubble injection: A numerical study focusing on bubble-bubble interaction," Physical Review E **76**(4), 046309.

Ilinskii, Y. A., Hamilton, M. F., and Zabolotskaya, E. A. (**2007**). "Bubble interaction dynamics in lagrangian and hamiltonian mechanics," The Journal of the Acoustical Society of America **121**(2), 786–795.

Katiyar, A., and Sarkar, K. (**2011**). "Excitation threshold for subharmonic generation from contrast microbubbles," The Journal of the Acoustical Society of America **130**(5), 3137–3147.

Keller, J. B., and Miksis, M. (**1980**). "Bubble oscillations of large amplitude," The Journal of the Acoustical Society of America **68**(2), 628–633.

Lauterborn, W., and Cramer, E. (**1981**). "Subharmonic route to chaos observed in acoustics," Physical Review Letters **47**(20), 1445.

Lauterborn, W., and Koch, A. (**1987**). "Holographic observation of period-doubled and chaotic bubble oscillations in acoustic cavitation," Physical Review A **35**(4), 1974.

Lauterborn, W., and Kurz, T. (**2010**). "Physics of bubble oscillations," Reports on progress in physics **73**(10), 106501.

Leroy, V., Strybulevych, A., Lanoy, M., Lemoult, F., Tourin, A., and Page, J. H. (**2015**). "Superabsorption of acoustic waves with bubble metascreens," Physical Review B **91**(2), 020301.

Leroy, V., Strybulevych, A., Scanlon, M., and Page, J. (**2009**). "Transmission of ultrasound through a single layer of bubbles," The European Physical Journal E **29**(1), 123–130.

Lohse, D. (**2018**). "Bubble puzzles: From fundamentals to applications," Physical review fluids **3**(11), 110504.

Lombard, O., Barrière, C., and Leroy, V. (**2015**). "Nonlinear multiple scattering of acoustic waves by a layer of bubbles," EPL (Europhysics Letters) **112**(2), 24002.

Maeda, K., and Colonius, T. (**2019**). "Bubble cloud dynamics in an ultrasound field," Journal of fluid mechanics **862**, 1105.

Manasseh, R., Nikolovska, A., Ooi, A., and Yoshida, S. (**2004**). "Anisotropy in the sound field generated by a bubble chain," Journal of Sound and Vibration **278**(4-5), 807–823.

Mettin, R., Akhatov, I., Parlitz, U., Ohl, C., and Lauterborn, W. (**1997**). "Bjerknes forces between small cavitation bubbles in a strong acoustic field," Physical review E **56**(3), 2924.

Miksis, M. J., and Ting, L. (**1989**). "Effects of bubbly layers on wave propagation," The Journal of the Acoustical Society of America **86**(6), 2349–2358.

Nio, A. Q., Faraci, A., Christensen-Jeffries, K., Raymond, J. L., Monaghan, M. J., Fuster, D., Forsberg, F., Eckersley, R. J., and Lamata, P. (**2019**). "Optimal control of sonovue microbubbles to estimate hydrostatic pressure," IEEE transactions on ultrasonics, ferroelectrics, and frequency control **67**(3), 557–567.

Okita, K., Sugiyama, K., Takagi, S., and Matsumto, Y. (**2013**). "Microbubble behavior in an ultrasound field for high intensity focused ultrasound therapy enhancement," The Journal of the Acoustical Society of America **134**(2), 1576–1585.

Ooi, A., Nikolovska, A., and Manasseh, R. (**2008**). "Analysis of time delay effects on a linear bubble chain system," The Journal of the Acoustical Society of America **124**(2), 815–826.

Pham, K., Mercier, J.-F., Fuster, D., Marigo, J.-J., and Maurel, A. (**2021**). "Scattering of acoustic waves by a nonlinear resonant bubbly screen," Journal of Fluid Mechanics **906**.

Prosperetti, A., Lezzi, A. *et al.* (**1986**). "Bubble dynamics in a compressible liquid. part 1. first-order theory.," J. FLUID MECH., 1986, **168**, 457–478.

Shampine, L. (**2005**). "Solving odes and ddes with residual control," Applied Numerical Mathematics **52**(1), 113–127.

Shampine, L. F. (**2008**). "Dissipative approximations to neutral ddes," Applied Mathematics and Computation **203**(2), 641–648.

516 Sujarittam, K., and Choi, J. J. (**2020**). "Angular dependence of the acoustic signal of a
517 microbubble cloud," The Journal of the Acoustical Society of America **148**(5), 2958–2972.
518 van't Wout, E., and Feuillade, C. (**2021**). "Proximity resonances of water-entrained air
519 bubbles near acoustically reflecting boundaries," The Journal of the Acoustical Society of
520 America **149**(4), 2477–2491.
521 Yasui, K., Iida, Y., Tuziuti, T., Kozuka, T., and Towata, A. (**2008**). "Strongly interacting
522 bubbles under an ultrasonic horn," Physical Review E **77**(1), 016609.
523 Ye, Z., and Feuillade, C. (**1997**). "Sound scattering by an air bubble near a plane sea
524 surface," The Journal of the Acoustical Society of America **102**(2), 798–805.